RESEARCH PAPER

CrossMark

Influence of alloy elements on microstructure and mechanical properties of Al/steel dissimilar joint by laser welding/brazing

Jin Yang[1] · Zhishui Yu[1] · Yulong Li[2] · Hua Zhang[2] · Wei Guo[3] · Norman Zhou[4]

Abstract

The problem in dissimilar material joining (e.g., Al/steel) is the degradation of joint mechanical properties by formation of the hard and brittle interfacial intermetallic compounds. In the present study, in order to improve the joint mechanical properties, alloy elements Si and Zn are added in the form of Al-Si and Zn-Al filler metals, respectively. The effects of alloy elements on the joints are investigated in terms of interfacial microstructure and mechanical properties. The results have shown that element Si is able to suppress the growth of interfacial reaction layer, which leads to the improvement in the fracture load, while element Zn is capable of reducing the brittleness of reaction layer, and it consequently enhances the fracture load.

Keywords Al/steel dissimilar joint · Microstructure · Mechanical properties · Laser welding/brazing

1 Introduction

Many welding studies have currently focused on dissimilar material welding. Dissimilar material joints have been used in vast applications due to their merits of weight reduction, energy efficiency, cost reduction, and optimization of material use. An increasing need in the automotive industry can be noted for dissimilar material joining of aluminum alloy and steel, because of the demands for the reduction of overall weight and the decrease in fuel consumption and carbon emission [1–3].

The joining of aluminum to steel is a great challenge due to the large differences in thermophysical properties between these two materials and especially the formation of inherently hard and brittle Fe-Al intermetallic compounds at elevated temperatures [4, 5]. In order to address this problem, many efforts have been made to control the formation and growth of Fe-Al IMCs in Al/steel joining in the past decades, such as optimizing process parameters [6, 7], applying advanced joining technologies [8, 9], and adopting alloy elements [10–22]. For instance, Si [10–15], Zn [16–19], Cu [20, 21], and Mg [22] are used as alloy elements in the forms of coating, interlayer, and filler metal, for manipulating the morphology and properties of the interfacial Fe-Al IMCs. However, a comparative study about influence of the alloy elements on the microstructure and mechanical properties of Al/steel joint is still lacking.

In this work, pure Al, AlSi$_{12}$, and ZnAl$_{22}$ filler metals were applied for Al/steel joining by using diode laser welding/brazing technology. The present study aims to investigate the influence of alloy elements on the microstructure and mechanical properties of laser dissimilar Al/steel joint.
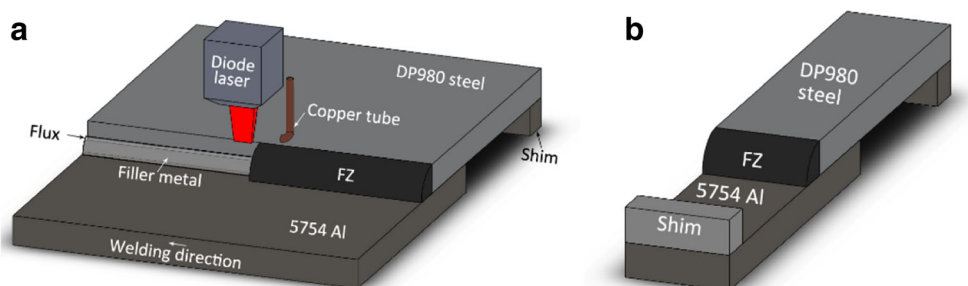
✉ Jin Yang
  jyang@sues.edu.cn

[1] Department of Materials Engineering, Shanghai University of Engineering Science, Shanghai 201620, China

[2] Key Laboratory of Robot and Welding Automation of Jiangxi Province, Nanchang University, Nanchang, Jiangxi 330031, China

[3] School of Mechanical Engineering and Automation, Beihang University, Beijing 100191, China

[4] Center for Advanced Materials Joining, University of Waterloo, Waterloo, ON N2L 3G1, Canada

2 Experimental

A diode laser was used to join 1.0-mm DP980 steel and 1.5-mm 5754 aluminum alloy in a lap joint configuration. The chemical composition of DP980 steel was 0.15Cr-2.1Mn-0.35Mo (wt.%); 5754 aluminum alloy was 2.6Mg-0.4Si-0.5Mn-0.4Fe (wt.%). 1100 pure Al, AlSi$_{12}$, and ZnAl$_{22}$ filler

metals with the diameters of 1.6 mm were used. A powder brazing flux, Superior No. 20, was applied.

Base materials were machined as rectangular strips of 50 × 60 mm^2. Specimens were sheared parallel to the rolling direction. The steel sheets were cleaned in acetone and then ground to 1000 grit using SiC abrasive paper and again ultrasonically cleaned in acetone. The aluminum alloy sheets went through a very strict two-step cleaning process, which was shown in our previous study [23].

An integrated Panasonic six-axis robot and a 4 kW Nuvonyx diode laser system were used for laser welding/brazing. A 1 × 12-mm^2 rectangular laser beam intensity profile was obtained at the focal point. The filler metal was placed on the surface of the steel sheet. To limit oxidation, shielding gas (99.99% Ar) was applied with a flow rate of 15 L/min from a 6-mm-diameter soft copper tube. A shim was placed below the aluminum sheet to minimize the gap between the faying surfaces. The experimental setup of laser welding/brazing is shown in Fig. 1a. The process parameters were 1.0–2.8 kW laser power, 0.2–1.0 m/min travel speed, 0-mm defocusing amount, and 0-mm deviation distance towards either side of base materials.

After the laser welding/brazing, to measure the mechanical properties of the joints, rectangular specimens were made from the joints and subjected to tensile-shear tests at room temperature with a crosshead speed of 1 mm/min. Shims were clamped to each end of the specimens to keep the joint interface parallel to the loading direction, as shown in Fig. 1b. The joint strength was presented as fracture load with the unit of newton (N) as the geometries of the tensile samples were not identical because of various fusion zone (FZ) geometries and complex stresses [24].

The specimens were cut across the joints to obtain cross sections to study the macrostructure and microstructure. Keller's reagent was used to reveal the microstructure of the sectioned joints. They were then observed using an Olympus BX51M optical microscope (OM). The microstructure and fracture morphology were analyzed using a JEOL JSM 6460 scanning electron microscope (SEM). The composition was determined using Oxford INCA energy-dispersive X-ray spectrometer (EDS). The FZ/steel interfacial phases were confirmed using a JEOL 2010F transmission electron microscope (TEM).

3 Results and discussion

3.1 Weld appearance and OM analysis

Figure 2a–c shows typical weld appearances of the laser joints with different filler metals. During laser irradiation, filler met-
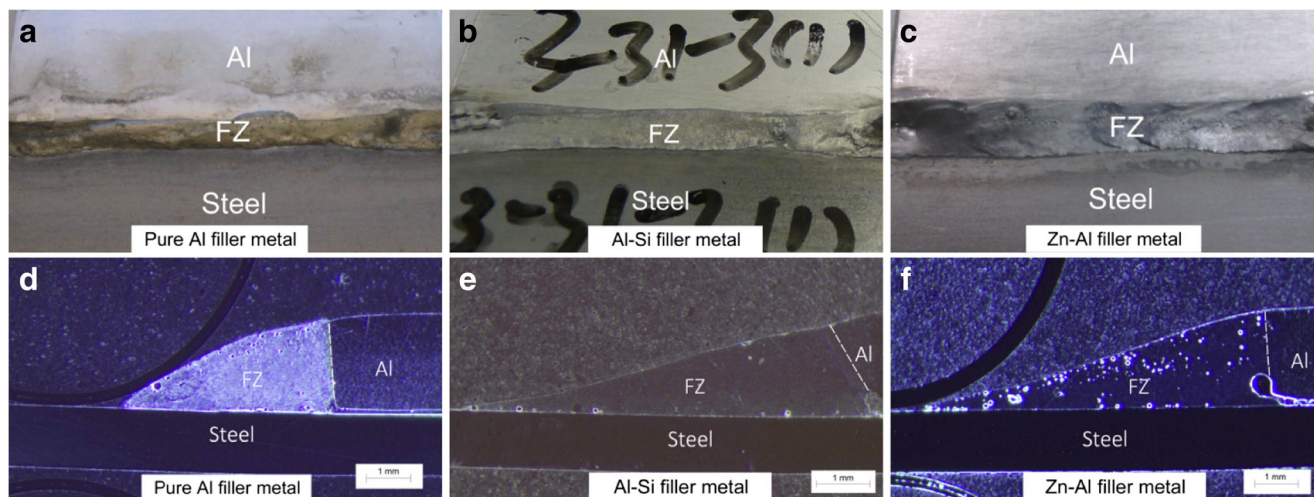

Fig. 2 Weld appearances and cross-sectional views of laser joints with different filler metals: a–c weld apperances, d–f cross sectional views
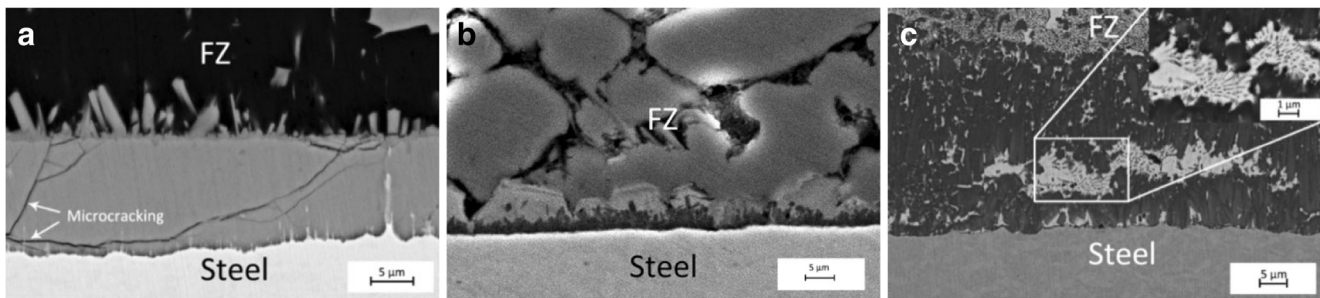
Fig. 3 SEM image of FZ/steel interfacial region in the laser Al/steel joints with different filler metals: **a** pure Al, **b** Al-Si, **c** Zn-Al

al melted, wetted, and spread on the steel surface, then solidified to form the FZ. As shown in Fig. 2a, when pure Al filler metal was used, non-uniform FZ was observed especially at the both ends of the specimen. In contrast, using Al-Si and Zn-Al filler metals resulted in uniform FZs with good wetting on both base materials (Fig. 2b, c). Figure 2d–f presents typical cross-sectional views of the laser joints with different filler metals. Comparing Fig. 2d to e and f, it was obvious that the FZ widths of latter ones were much larger than that of the former one, which indicated better wetting on the steel substrate when using Al-Si and Zn-Al filler metals.

3.2 SEM analysis

Figure 3 shows SEM images of typically interfacial microstructure of laser Al/steel joints with different filler metals. In the case of pure Al filler metal, the interfacial reaction layer was mainly composed of two phases, i.e., needle-like phase adjacent to FZ and lamellar phase adjacent to steel (Fig. 3a). Based on the EDS analysis, the needle-like phase had the chemical composition of 72.6Al-27.4Fe (at. %), while the lamellar structure phase had the chemical composition of 78.3Al-21.7Fe (at. %). Thus, the needle-like phase and lamellar phase were identified as $FeAl_3$ and Fe_2Al_5, respectively. Besides, microcracking was observed in Fe_2Al_5 layer. Figure 3b presents the SEM image of laser Al/steel joint with Al-Si filler metal. An island-shaped phase at the FZ side and a bumpy

phase at the steel side were observed. Based on the EDS analysis, the chemical composition of the island-shaped phase was 74.7Al-8.7Si-16.6Fe (at. %), while the chemical composition of the bumpy phase was 70.9Al-5.5Si-23.6Fe (at. %). Therefore, the island-shaped and bumpy phases were identified as $Al_{7.2}Fe_{1.8}Si$ and $Fe(Al,Si)_3$, respectively. Figure 3c shows the backscattered electron (BSE) image of typically interfacial microstructure of laser Al/steel joint with Zn-Al filler metal. The reaction layer consisted of a dark layered structure, a light dispersed structure, and a gray stripy structure. The EDS analysis showed that the layered structure contained 64.3Al-30.3Fe-5.4Zn (at. %), while the dispersed structure contained 8.7Al-6.0Fe-85.3Zn (at. %). According to the Fe-Al-Zn ternary phase diagram, the possible phases of layered and dispersed structures were $Fe_2Al_{5-x}Zn_x$ and $FeZn_{10}$, respectively. It is noted that the gray stripy structure is too small to be accurately measured by SEM-EDS (the inset in Fig. 3c), and this structure will be characterized by TEM analysis.

3.3 TEM analysis

Figure 4 shows TEM analysis of the laser joint with Al-Si filler metal. In the bright filed (BF) image, some dark $Fe(Al,Si)_3$ particles were formed inside a hexagonal $Al_{7.2}Fe_{1.8}Si$. Figure 4b, c shows the selected area diffraction patterns (SADPs), which represent the incident beams parallel to $[\bar{1}2\bar{1}1]_{Al7.2Fe1.8Si}$ and $[0\bar{2}1]_{Fe(Al,Si)3}$ zone axes.
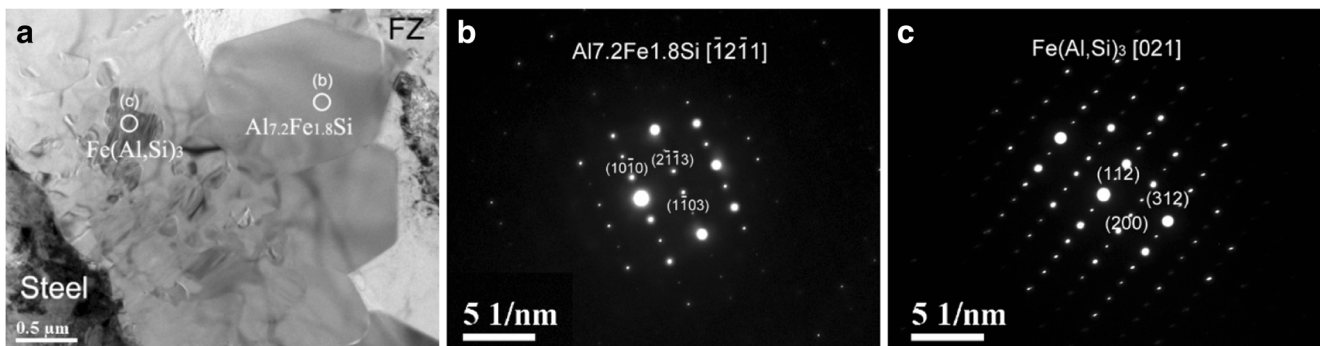

Fig. 4 TEM analysis of the laser joint with Al-Si filler metal: **a** BF image, **b** and **c** SADPs of $Al_{7.2}Fe_{1.8}Si$ and $Fe(Al,Si)_3$
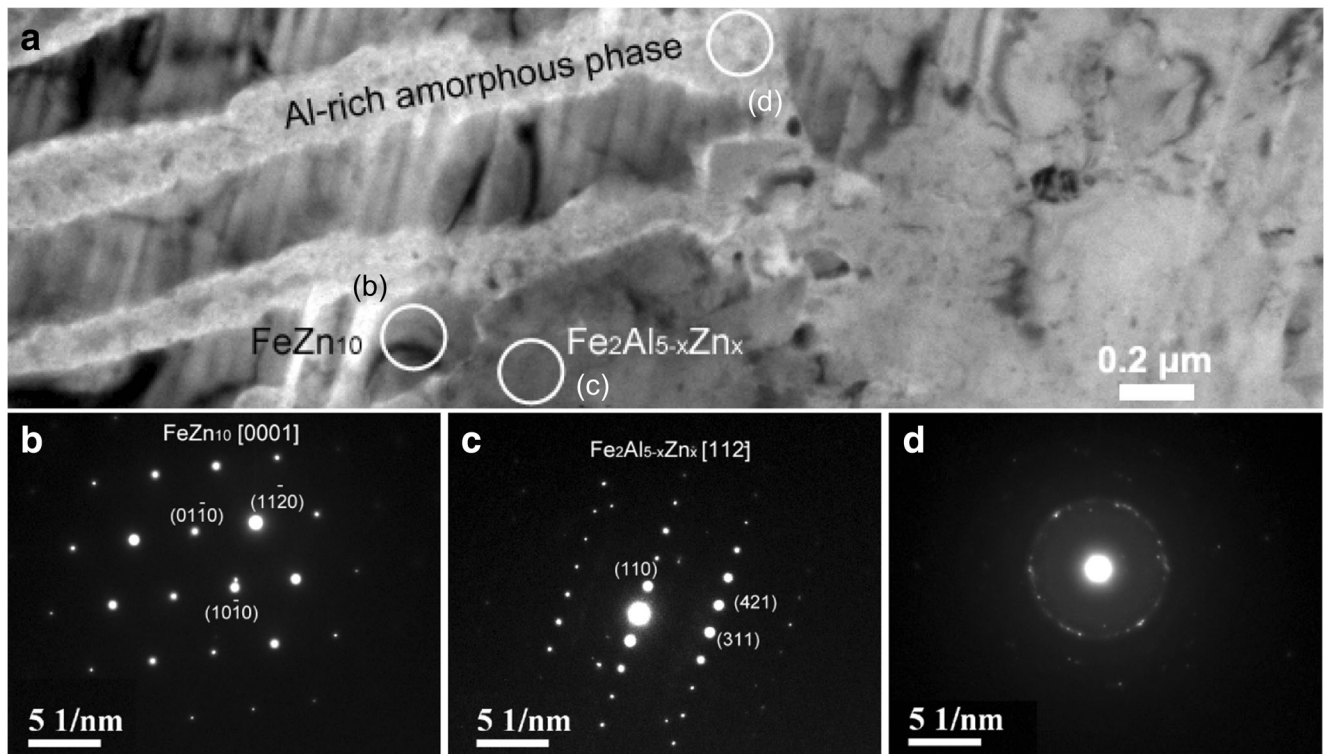
Fig. 5 TEM analysis of the laser joint with Zn-Al filler metal: **a** BF image, **b, c,** and **d** SADPs of FeZn$_{10}$, Fe$_2$Al$_{5-x}$Zn$_x$ and Al-rich amorphous phase, respectively

Figure 5 displays the TEM analysis of the laser joint with Zn-Al filler metal. Figure 5b, c presents the SADPs of the interfacial phases, which represent the incident beams $[\bar{1}12]_{\text{Fe2Al5}-x\text{Znx}}$ and $[0001]_{\text{FeZn10}}$ zone axes. The gray stripy structures in the BSE image (Fig. 3c) presented to be a light lath structures in BF image (Fig. 5a). The SADPs of this structure showed a strong amorphous halo (Fig. 5d). Besides, based on the TEM-EDS analysis, it contained 56.6Al-1.0Fe-42.4Zn (at. %), which was reasonably determined to be an Al-rich amorphous phase.

3.4 Fracture load and fracture behavior

The fracture load vs the variety of filler metal and joint failure mode is displayed in Fig. 6. When pure Al filler metal was used, the fracture load was 727 N and the joint failed at the interfacial region. When Al-Si filler metal was used, the fracture load increased to 1085 N and the joint failed near the FZ. With the similar failure location, the fracture load slightly increased to 1233 N when Zn-Al filler metal was applied.

Figure 7 compiles the failure joint with pure Al filler metal and fracture surface morphologies. As shown in Fig. 7a, the fracture occurred at the FZ/steel interface. Figure 7b, c displays a mass of river patterns and tearing ridges on the fracture surfaces, indicating a cleavage brittle failure. Based on the EDS analysis, Fe$_2$Al$_5$ was detected on both sides of the fracture surfaces. It suggested that the fracture occurred inside Fe$_2$Al$_5$ layer which was due to the formation of microcracking in this region (Fig. 3a).
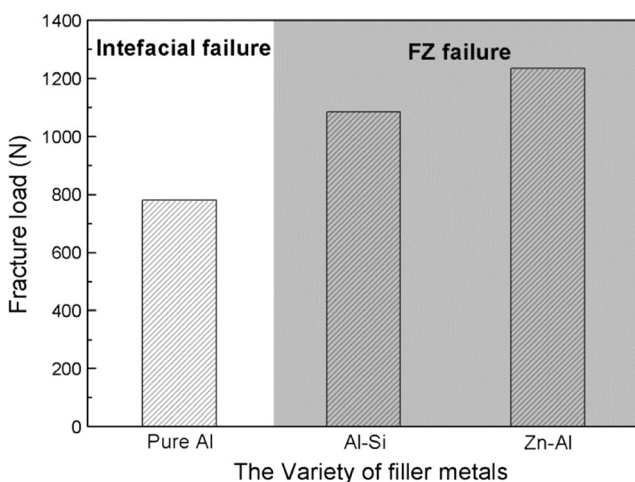

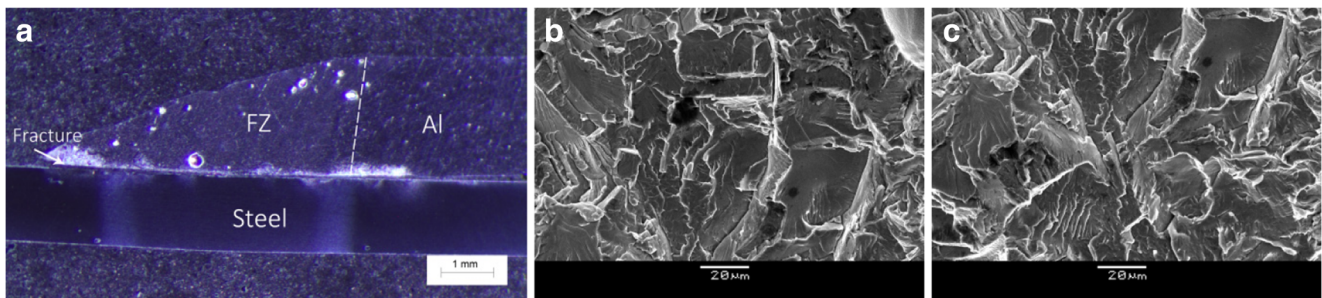Fig. 6 Fracture load vs the variety of filler metal and joint failure mode

Fig. 7 Failure joint with pure Al filler metal and fracture surface morphologies: **a** failure joint, **b** and **c** fracture surfaces at the FZ side and the steel side, respectively
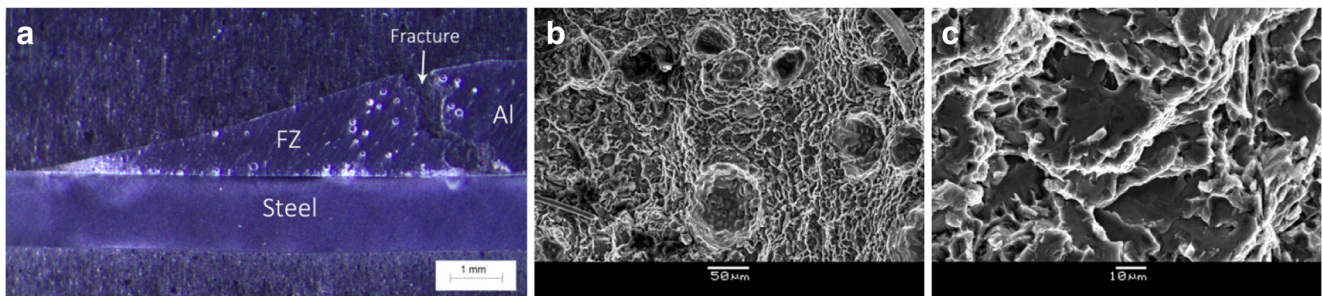

Fig. 8 Failure joint with Al-Si filler metal and fracture surface morphologies: **a** failure joint, **b** and **c** fracture surfaces at the FZ side and the Al side, respectively

Figure 8 presents the failure joint with Al-Si filler metal and fracture surface morphologies. The fracture located at the FZ/Al interface as shown in Fig. 8a. A mixture of smooth planes and river patterns were seen on the fracture surfaces which was the characteristic of brittle cleavage failure (Fig. 8b, c). Based on the EDS analysis, α-Al, Al-Si eutectic, and Al5FeSi were detected, which indicated that the fracture mainly occurred in the FZ.

Figure 9 shows the failure joint with Zn-Al filler metal and fracture surface morphologies. Similar to the case of Al-Si filler metal, the fracture was observed near the FZ/Al interface (Fig. 9a). Figure 9b, c displays the ductile failure with a large amount of uniform dimples. Based on the EDS analysis, α-Al

containing a few amount of Mg was detected, suggesting an Al heat-affected zone (HAZ) fracture.

3.5 Influence of alloy elements

The changes of fracture load and fracture behavior can be correlated to the change of interfacial microstructure. In the case of pure Al filler metal, the reaction layer is as thick as 12 μm (Fig. 3a). Besides, the microhardness of $FeAl_3$ and Fe_2Al_5 are up to 892 and 1013 HV, respectively [4]. These combined factors significantly embrittle the joint and lead to low fracture load and the interfacial failure. In the case of Al-
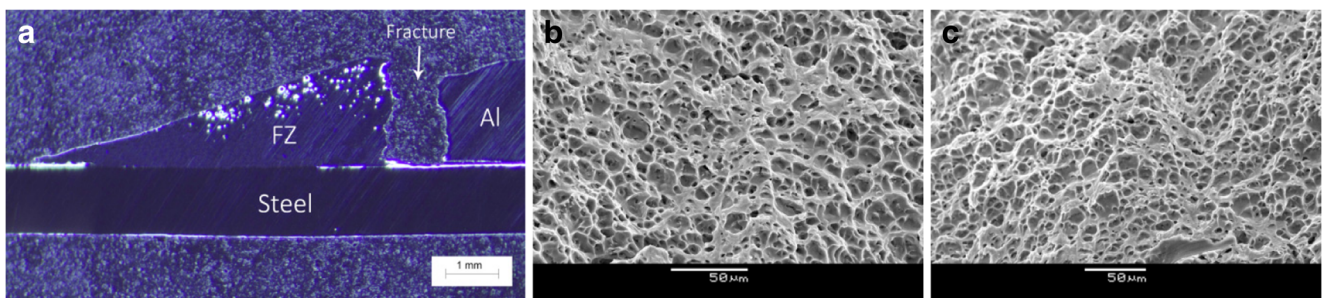

Fig. 9 Failure joint with Zn-Al filler metal and fracture surface morphologies: **a** failure joint, **b** and **c** fracture surface at the FZ side and the Al side, respectively

Si filler metal, the microhardness values of $Al_{7.2}Fe_{1.8}Si$ and $Fe(Al,Si)_3$ are 956 and 883 HV, respectively [23], which are similar to the case of pure Al filler metal. However, the thickness of reaction layer reduces to 8 μm (Fig. 3b). Thus, it suggests that alloy element Si is able to suppress the growth of reaction layer. With the thinned reaction layer, the fracture load is thus improved. In the case of Zn-Al filler metal, the thickness of reaction layer is increased to 38 μm (Fig. 2c). Surprisingly, it is opposed to many previous findings that the thinner the reaction layer indicates the higher fracture load [10, 11]. It is noted that the nanohardness values of $Fe_2Al_{5-x}Zn_x$ and $FeZn_{10}$ are 3.05 and 11.52 GPa, respectively, which are converted to 311 and 1175 HV [25]. Apparently, the average hardness (brittleness) of the reaction layer is much lower than that of with pure Al filler metal. Thus, it infers that the reduction in brittleness of the reaction layer is responsible for the enhancement in the fracture load.

4 Conclusion

Dissimilar Al/steel joints were successfully produced by laser welding/brazing using pure Al, Al-Si, and Zn-Al filler metals. By comparing the laser joints with different filler metals, the influence of alloy elements Si and Zn on microstructure and mechanical properties was investigated. The major conclusions can be summarized as follows:

1. For the pure Al filler metal, a 12-μm-thick reaction layer consisted of $FeAl_3$ and Fe_2Al_5 is formed at the FZ/steel interface. Microcracking is observed in the layer of Fe_2Al_5. The joint fracture load is 727 N, and joint fails at the Fe_2Al_5 layer.
2. For the Al-Si filler metal, $Al_{7.2}Fe_{1.8}Si$ and $Fe(Al,Si)_3$ reaction layers with the total thickness of 8 μm are observed at the interfacial region. The joint fracture load is 1085 N, and the failure location is at the FZ.
3. For the Zn-Al filler metal, the reaction layer consists of $Fe_2Al_{5-x}Zn_x$, $FeZn_{10}$, and small amount of Al-rich amorphous phase. Thickness of the reaction layer is 38 μm. The joint fracture load is 1233 N and joint fails at the Al HAZ.
4. Element Si is able to suppress the growth of interfacial reaction layer, which leads to the fracture load improvement, while element Zn is capable of reducing the brittleness of reaction products, and it consequently enhances the fracture load.

References

1. Rendigs KH (1996) Aluminium structures used in aerospace-status and prospects. Mater Sci Forum 242:11–24. https://doi.org/10.4028/www.scientific.net/msf.242.11
2. Chen S, Daehn GS, Vivek A (2016) Interfacial microstructures and mechanical property of vaporizing foil actuator welding of aluminum alloy to steel. Mater Sci Eng A 659:12–21. https://doi.org/10.1016/j.msea.2016.02.040
3. Z. Zeng, J.P. Olive, M. Yang, D. Song and B. Peng(2017) Functional fatigue behaviour of NiTi-Cu dissimilar laser welds, 114, 282–287. https://doi.org/10.1016/j.matdes.2016.11.023
4. Rathod MJ, Kutsuna M (2004) Joining of aluminum alloy 5052 and low-carbon steel by laser roll welding. Welding J 83:16s–24s
5. Torkamany MJ, Tahamtan S, Sabbaghzadeh J (2010) Dissimilar welding of carbon steel to 5754 aluminum alloy by Nd: YAG pulsed laser. Mater Des 31(1):458–465. https://doi.org/10.1016/j.matdes.2009.05.046
6. Tran VX, Pan J (2010) Fatigue behavior of dissimilar spot friction welds in lap-shear and cross-tension specimens of aluminum and steel sheets. Int J Fatigue 32(7):1167–1179. https://doi.org/10.1016/j.ijfatigue.2009.12.011
7. Acarer M, Demir B (2008) An investigation of mechanical and metallurgical properties of explosive welded aluminum–dual phase steel. Mater Lett 62(25):4158–4160. https://doi.org/10.1016/j.matlet.2008.05.060
8. Kimura M, Ishii H, Kusaka M, Kaizu K, Fuji A (2009) Joining phenomena and fracture load of friction welded joint between pure aluminium and low carbon steel. Sci Technol Weld Join 14(5):388–395. https://doi.org/10.1179/136217109X425856
9. Ding Y, Shen Z, Gerlich AP (2017) Refill friction stir spot welding of dissimilar aluminum alloy and AlSi coated stee. J Manuf Process 30:353–360. https://doi.org/10.1016/j.jmapro.2017.10.006
10. Song JL, Lin SB, Yang CL, Fan CL (2009) Effects of Si additions on intermetallic compound layer of aluminum-steel TIG welding-brazing joint. J Alloys Compd 488(1):217–222. https://doi.org/10.1016/j.jallcom.2009.08.084
11. Cao R, Yu G, Chen JH, Wang PC (2013) Cold metal transfer joining aluminum alloys-to-galvanized mild steel. J Mater Process Technol 213(10):1753–1763. https://doi.org/10.1016/j.jmatprotec.2013.04.004
12. Saida K, Song W, Nishimoto K (2005) Diode laser brazing of aluminium alloy to steels with aluminium filler metal. Sci Technol Weld Join 10(2):227–235. https://doi.org/10.1179/174329305X37060
13. Su Y, Hua X, Wu Y (2014) Quantitative characterization of porosity in Fe-Al dissimilar materials lap joint made by gas metal arc welding with different current modes. J Mater Process Technol 214(1):81–86. https://doi.org/10.1016/j.jmatprotec.2013.08.002
14. Zhang HT, Feng JC, He P, Hackl H (2007) Interfacial microstructure and mechanical properties of aluminium-zinc-coated steel joints made by a modified metal inert gas welding-brazing process. Mater Charact 58(7):588–592. https://doi.org/10.1016/j.matchar.2006.07.008
15. Li L, Xia H, Tan CW, Ma N (2018) Effect of groove shape on laser welding-brazing Al to steel. J Mater Process Technol 252:573–581. https://doi.org/10.1016/j.jmatprotec.2017.10.025
16. Dong H, Yang L, Dong C, Kou S (2010) Arc joining of aluminum alloy to stainless steel with flux-cored Zn-based filler metal. Mater Sci Eng A 527(26):7151–7154. https://doi.org/10.1016/j.msea.2010.07.092
17. Mathieu A, Shabadi R, Deschamps A, Suery M, Matteï S, Grevey D, Cicala E (2007) Dissimilar material joining using laser (aluminum to steel using zinc-based filler wire). Opt

Laser Technol 39(3):652–661. https://doi.org/10.1016/j.optlastec.2005.08.014

18. Sierra G, Peyre P, Beaume FD, Stuart D, Fras G (2008) Steel to aluminium braze welding by laser process with Al–12Si filler wire. Sci Technol Weld Join 13(5):430–437. https://doi.org/10.1179/174329308X341852

19. Dharmendra C, Rao KP, Wilden J, Reich S (2011) Study on laser welding–brazing of zinc coated steel to aluminum alloy with a zinc based filler. Mater Sci Eng A 528(3):1497–1503. https://doi.org/10.1016/j.msea.2010.10.050

20. Lin SB, Song JL, Yang CL, Fan CL, Zhang DW (2010) Brazability of dissimilar metals tungsten inert gas butt welding-brazing between aluminum alloy and stainless steel with Al-Cu filler metal. Mater Des 31(5):2637–2642. https://doi.org/10.1016/j.matdes.2009.12.005

21. Dong H, Hu W, Duan Y, Wang X, Dong C (2012) Dissimilar metal joining of aluminum alloy to galvanized steel with Al-Si, Al-Cu, Al-Si-Cu and Zn-Al filler wires. J Mater Process Technol 212(2):458–464. https://doi.org/10.1016/j.jmatprotec.2011.10.009

22. Su Y, Hua X, Wu Y (2014) Influence of alloy elements on microstructure and mechanical property of aluminum–steel lap joint made by gas metal arc welding. J Mater Process Technol 214(4):750–755. https://doi.org/10.1016/j.jmatprotec.2013.11.022

23. Yang J, Li YL, Zhang H, Guo W, Weckman D, Zhou N (2015) Dissimilar laser welding/brazing of 5754 aluminum alloy to dp 980 steel: mechanical properties and interfacial microstructure. Metall Mater Trans A 46(11):5149–5157. https://doi.org/10.1007/s11661-015-3079-x

24. Chen SH, Huang JH, Yang DD, Ma K, Zhang H (2012) The effect of Ni foil interlayer on laser key-hole welding of stainless steel to aluminum alloy. Trans China Weld Inst 33:9–12

25. Yang J, Li YL, Zhang H, Guo W, Zhou Y (2015) Control of interfacial intermetallic compounds in Fe-Al joining by Zn addition. Mater Sci Eng A 645:323–327. https://doi.org/10.1016/j.msea.2015.08.036